The Sensitivity to Basis Mismatch of Compressed Sensing for Spectrum Analysis and Beamforming

Yuejie Chi,[1] Louis Scharf,[2] Ali Pezeshki,[2] and Robert Calderbank[1]
[1]*Department of Electrical Engineering, Princeton University*
Princeton, NJ 08544, USA
[2]*Department of Electrical and Computer Engineering, Colorado State University*
Fort Collins, CO 80523, USA

***Abstract*—The theory of compressed sensing suggests that successful inversion of an image of the physical world (e.g., a radar/sonar return or a sensor array snapshot vector) for the source modes and amplitudes can be achieved at measurement dimensions far lower than what might be expected from the classical theories of spectrum or modal analysis, provided that the image is sparse in an *apriori known* basis. For imaging problems in passive and active radar and sonar, this basis is usually taken to be a DFT basis. The compressed sensing measurements are then inverted using an ℓ_1-minimization principle (basis pursuit) for the nonzero source amplitudes. This seems to make compressed sensing an ideal image inversion principle for high resolution modal analysis. However, in reality no physical field is sparse in the DFT basis or in an apriori known basis. In fact the main goal in image inversion is to *identify* the modal structure. No matter how finely we grid the parameter space the sources may not lie in the center of the grid cells and there is always mismatch between the assumed and the actual bases for sparsity.**

In this paper, we study the sensitivity of basis pursuit to mismatch between the assumed and the actual sparsity bases and compare the performance of basis pursuit with that of classical image inversion. Our mathematical analysis and numerical examples show that the performance of basis pursuit degrades considerably in the presence of mismatch, and they suggest that the use of compressed sensing as a modal analysis principle requires more consideration and refinement, at least for the problem sizes common to radar/sonar.

I. Introduction

Broadly speaking there are two main (classical) principles for inverting the kinds of images that are measured in radar, sonar, and optics. The first principle is one of matched filtering, wherein a sequence of test images is matched to the measured image. The test images are generated by scanning a prototype image (e.g., a waveform or a steering vector) through frequency, wavenumber, doppler, and/or delay. In time series analysis, this amounts to classical spectrum analysis to identify the frequency modes, and the corresponding mode amplitudes, of the signal [1]. In phased-array processing, it amounts to spectrum analysis in frequency and wavenumber to identify the frequency-wavenumber coordinates of sources impinging on the array [2]. In Space-Time Adaptive Processing (STAP) radar and sonar, it amounts to spectrum analysis in delay, frequency, and wavenumber to reconstruct the radar/sonar field [3],[4]. The second principle is one of parameter estimation in a separable linear model, wherein a sparse *modal* representation for the field is posited and estimates of linear parameters (complex amplitudes of modes) and nonlinear mode parameters (frequency, wavenumber, delay, and/or doppler) are extracted, usually based on maximum likelihood, or some variation on linear prediction, using l_2 minimization (cf. [5]). There is a comprehensive literature in electrical engineering, physics, and chemistry on the performance and limitations of these two classical principles (cf. [1],[5]–[8]). One important limitation is that any subsampling of the measured image has consequences for resolution (or bias) and for variability (or variance).

The recent advent of compressed sensing theory (cf. [9]–[11]) has created a great deal of enthusiasm among the signal processing community, as it suggests that subsampling (actually *subrecording*) has manageable consequences for image inversion, provided that the image is sparse in an *apriori known* basis. For imaging problems in passive and active radar and sonar, this basis is usually taken to be a Fourier basis (actually a DFT basis) constructed for resolution of $2\pi/N$, with N a window length, array length, or pulse-to-pulse processing length. Several articles (see for example [12]–[14]) consider the use of compressed sensing theory for radar and sonar imaging when the targets are taken to be on a regular grid in delay, Doppler, and wavenumber, and advocate this theory as a new high resolution imaging principle. But no matter how large the size N of the grid is, the actual field will not place its targets on the center of the grid points $\{2\pi n/N\}$ in frequency or wavenumber, or on the center of the grid points in delay-Doppler-wavenumber. This means the image is actually *not sparse* in the DFT basis or the basis defined by the grid. In fact any target that lies between two cells of a discretely-resolved range-doppler plane or frequency-wavenumber plane will spill non-zero values into all cells, with the amplitude of the spillage following a Lanczos kernel, decaying as $1/f$, where f is frequency or wavenumber. This observation raises the following questions.

1) What is the sensitivity of compressed sensing for modal analysis (image inversion as opposed to image reconstruction) to *mismatch* between the assumed basis for sparsity and the actual basis in which the image is sparse?

2) How does the performance of compressed sensing in the presence of basis mismatch compare with the performance of classical matched filtering for imaging in frequency, wavenumber, delay, and/or doppler, or with that of linear prediction?

This paper was presented at the sixth Defense Applications of Signal Processing (DASP) workshop in Lihue, HI, USA, September 2009.

In this paper, we aim to answer these questions for problems typical of spectrum analysis and beamforming. In order to frame them more precisely, let us begin with two models for a measured image $\mathbf{s} \in \mathbb{C}^N$. In the mathematical model, to be *assumed* in the compressed sensing procedure, the image is composed as $\mathbf{s} = \mathbf{\Psi}_0 \mathbf{x}$, where $\mathbf{\Psi}_0 \in \mathbb{C}^{N \times N}$ is known, and typically a gridded imaging matrix (e.g., the N point DFT matrix), and $\mathbf{x} \in \mathbb{C}^N$ is a sparse or compressible vector[1] of field parameters that compose the image as a linear combination of columns of $\mathbf{\Psi}_0$. But, as a matter of fact, the image $\mathbf{s}$ is composed by the physics as $\mathbf{s} = \mathbf{\Psi}_1 \boldsymbol{\theta}$, where $\mathbf{\Psi}_1 \in \mathbb{C}^{N \times N}$ is determined by a point spread function, a Green's function, or an impulse response, and the field parameter vector $\boldsymbol{\theta}$ is sparse. Typically $\mathbf{\Psi}_1$ is determined by frequency, wavenumber, delay, and/or doppler parameters that are *unknown* apriori. More importantly, these parameters do *not* lie exactly on the gridding points of $\mathbf{\Psi}_0$, e.g. a DFT matrix or an identity matrix. So $\mathbf{\Psi}_0 \neq \mathbf{\Psi}_1$. We call this basis mismatch, and note that it is present in all imaging problems, no matter how large N is, or equivalently no matter how fine-grained the gridding procedure is.

Each of the hypothesized models for the image $\mathbf{s}$ may be inverted for its field parameters:

$$\mathbf{x} = \mathbf{\Psi}_0^{-1}\mathbf{s} \quad \text{and} \quad \boldsymbol{\theta} = \mathbf{\Psi}_1^{-1}\mathbf{s} \tag{1}$$

These inversions[2] determine the coordinate transformation

$$\mathbf{x} = \mathbf{\Psi}\boldsymbol{\theta} \quad \text{and} \quad \boldsymbol{\theta} = \mathbf{\Psi}^{-1}\mathbf{x} \tag{2}$$

where $\mathbf{\Psi} = \mathbf{\Psi}_0^{-1}\mathbf{\Psi}_1 \in \mathbb{C}^{N \times N}$.

If $\mathbf{s}$ is sparse in $\mathbf{\Psi}_1$, as is typical in spectrum analysis, beamforming, and range-doppler imaging, then the field parameters $\boldsymbol{\theta}$ will be sparse in the $\mathbf{I}$ basis. The field parameters $\mathbf{x} = \mathbf{\Psi}\boldsymbol{\theta}$ will be sparse in the $\mathbf{\Psi}$ basis, *but not in the identity basis*. So the question is, "what is the consequence of assuming that $\mathbf{x}$ is sparse in $\mathbf{I}$, when in fact it is only sparse in an *unknown* basis $\mathbf{\Psi}$, which is determined by the mismatch between $\mathbf{\Psi}_0$ and $\mathbf{\Psi}_1$?"

We answer this question by deriving bounds on the ℓ_1-norm (and also the ℓ_2-norm) of the error in reconstructing the actual sparse parameter vector $\boldsymbol{\theta}$ from its compressed sensing measurements using basis pursuit. In particular, we show that the upper bound for the ℓ_1-norm of the reconstruction error grows linearly with $N\epsilon\|\boldsymbol{\theta}\|_1$, where ϵ upper bounds the element-wise mismatch between $\mathbf{\Psi}$ and $\mathbf{I}$. We substantiate our mathematical analysis by presenting numerical examples that demonstrate a considerable performance degradation for image inversion using compressed sensing, when the assumed basis is a DFT basis but the actual basis has elements between DFT points. The inaccuracy in field reconstruction persists even when the number of compressed sensing measurements is increased to the full image dimension. Comparisons show that classical approaches, in particular linear prediction, can provide more reliable reconstructions of the field than basis pursuit in the presence of basis mismatch.

Our results suggest that the hope that a small number of recordings can be processed according to the principles of compressed sensing to produce the performance of classical methods that use a large number of samples seems to be unattainable due to the inevitable mismatch between the sparsity basis assumed by compressed sensing and the actual sparsity basis selected by the physical world. It is this mismatch problem that moderates our enthusiasm for compressed sensing as a high resolution image inversion principle, at least for problem sizes typical in radar/sonar and spectrum analysis.

This paper is a summary of results. We have omitted the proofs, and derivations have been shortened or left out entirely. A comprehensive treatment along with detailed proofs is presented in [15].

II. Basis mismatch

There are two steps in the procedure of compressed sensing, namely compressed recording and inversion for parameters (cf. [9]–[11]). In recording, we make linear measurements of $\mathbf{s}$, with possible additive noise $\mathbf{b}$, so the observation $\mathbf{y}$ is

$$\mathbf{y} = \mathbf{\Phi}\mathbf{s} + \mathbf{b} = (\mathbf{\Phi}\mathbf{\Psi}_0)\mathbf{x} + \mathbf{b} \triangleq \mathbf{A}\mathbf{x} + \mathbf{b} \tag{3}$$

where $\mathbf{\Phi} \in \mathbb{C}^{M \times N}$ is the compressed sensing measurement matrix (typically a matrix with i.i.d. Gaussian or i.i.d Bernoulli entries), and M is the number of measurements. We now define $\mathbf{A} = \mathbf{\Phi}\mathbf{\Psi}_0 \in \mathbb{C}^{M \times N}$ as the new measurement matrix with respect to $\mathbf{x}$. Without loss of generality, we will only deal with $\mathbf{A}$ and $\mathbf{\Psi}$ in the following discussions.

In reconstruction, we seek the sparsest solution to $\mathbf{x}$ given the observation $\mathbf{y}$. For noise-free case ($\mathbf{b} = \mathbf{0}$), we wish to solve

$$\mathbf{x}^* = \arg\min_{\mathbf{x}} \|\mathbf{x}\|_0 \quad s.t. \quad \mathbf{y} = \mathbf{A}\mathbf{x}. \tag{4}$$

This is in general an NP-hard problem. However, if the measurement matrix $\mathbf{A}$ satisfies the so-called restricted isometry property (RIP) [16],[17] the solution to (4) can be obtained using linear programming, equivalent to the following ℓ_1 minimization problem:

$$\mathbf{x}^* = \arg\min_{\mathbf{x}} \|\mathbf{x}\|_1 \quad s.t. \quad \mathbf{y} = \mathbf{A}\mathbf{x}. \tag{5}$$

This is referred to as basis pursuit. In the noisy case, the problem is modified as:

$$\mathbf{x}^* = \arg\min_{\mathbf{x}} \|\mathbf{x}\|_1 \quad s.t. \quad \|\mathbf{y} - \mathbf{A}\mathbf{x}\|_2 \leq \epsilon \tag{6}$$

when $\|\mathbf{b}\|_2 \leq \epsilon$ is the bounded noise.

From [16],[17], when the restricted isometry constant (RIC) of the measurement matrix $\mathbf{A}$ satisfies $\delta_{2k}^{\mathbf{A}} < \sqrt{2} - 1$ for $2k$-sparse signals, the solution $\mathbf{x}^*$ to (5) obeys

$$\|\mathbf{x}^* - \mathbf{x}\|_1 \leq C_0 \|\mathbf{x} - \mathbf{x}_k\|_1 \tag{7}$$

[1] If $\mathbf{x}$ is sparse, then the cardinality of its support $T_{\mathbf{x}} = \{k : x_k \neq 0\}$ is assumed to be small. If $\mathbf{x}$ is compressible, then its entries obey a power law i.e. the kth largest entry of absolute values satisfies $|x|_{(k)} \leq C_r \cdot k^{-r}$, $r > 1$ and C_r is a constant depending only on r, then $\|\mathbf{x} - \mathbf{x}_k\|_1 \leq \sqrt{k} C_r' \cdot k^{-r+1}$, where $\mathbf{x}_k$ is the k-term approximation of $\mathbf{x}$.

[2] If $\mathbf{\Psi}_0 \in \mathbb{C}^{L \times N}$ and $\mathbf{\Psi}_1 \in \mathbb{C}^{L \times N}$, with $L < N$, are overcomplete dictionaries then $\mathbf{s} \in \mathbb{C}^L$ and the inverses in (1) and (2) are replaced with pseudo Moore-Penrose pseudo inverses $\mathbf{\Psi}_0^\dagger = \mathbf{\Psi}_0^H(\mathbf{\Psi}_0\mathbf{\Psi}_0^H)^{-1}$ and $\mathbf{\Psi}_1^\dagger = \mathbf{\Psi}_1^H(\mathbf{\Psi}_1\mathbf{\Psi}_1^H)^{-1}$. However, throughout the paper we assume, without loss of generality, that $L = N$, having in mind that the developments also apply to the case where $L < N$.

and

$$\|\mathbf{x}^* - \mathbf{x}\|_2 \leq C_0 k^{-1/2} \|\mathbf{x} - \mathbf{x}_k\|_1 \tag{8}$$

where $\mathbf{x}_k$ is the k-term approximation of $\mathbf{x}$. For the noisy case (6), we have

$$\|\mathbf{x}^* - \mathbf{x}\|_2 \leq C_0 k^{-1/2} \|\mathbf{x} - \mathbf{x}_k\|_1 + C_1 \epsilon. \tag{9}$$

In addition, let

$$\alpha = \frac{2\sqrt{1+\delta_{2k}^{\mathbf{A}}}}{1-\delta_{2k}^{\mathbf{A}}} \quad \text{and} \quad \beta = \frac{\sqrt{2}\delta_{2k}^{\mathbf{A}}}{1-\delta_{2k}^{\mathbf{A}}}, \tag{10}$$

then the constants C_0 and C_1 satisfy

$$C_0 = \frac{2(1+\beta)}{1-\beta} \quad \text{and} \quad C_1 = \frac{2\alpha}{1-\beta}. \tag{11}$$

In the matched case where the hypothesized basis $\mathbf{\Psi}_0$ coincides with the actual basis $\mathbf{\Psi}_1$, the mismatched basis $\mathbf{\Psi} = \mathbf{\Psi}_0^{-1}\mathbf{\Psi}_1$ reduces to $\mathbf{I}$ and $\mathbf{x} = \boldsymbol{\theta}$ is sparse in the $\mathbf{I}$ basis. If $\boldsymbol{\theta}$ is k-sparse, the bound $\|\mathbf{x} - \mathbf{x}_k\|_1$ is zero in (7) and the solution $\mathbf{x}^*$ to $\mathbf{x}$ is exact in the noise-free case.

However, in the mismatched case where $\mathbf{\Psi}_0 \neq \mathbf{\Psi}_1$, $\mathbf{x} = \mathbf{\Psi}\boldsymbol{\theta}$ is actually sparse in the $\mathbf{\Psi}$ basis, rather than sparse in the $\mathbf{I}$ basis. So the question is, "what is the consequence of minimizing $\|\mathbf{x}\|_1$ under the constraint $\mathbf{y} = \mathbf{A}\mathbf{x}$, when in fact the correct minimization is to minimize $\|\boldsymbol{\theta}\|_1$ under the constraint $\mathbf{y} = \mathbf{A}\mathbf{\Psi}\boldsymbol{\theta}$ where $\mathbf{A} = \mathbf{\Phi}\mathbf{\Psi_0}$?"

We answer this question by analyzing the ℓ_1 error bound $\|\mathbf{x}^* - \boldsymbol{\theta}\|_1$ and ℓ_2 error bound $\|\mathbf{x}^* - \boldsymbol{\theta}\|_2$ under certain conditions on the mismatch basis $\mathbf{\Psi}$. The k-term approximation error bound $\|\mathbf{x} - \mathbf{x}_k\|_1$ in the presence of mismatch is central to the analysis.

Remark: Our analysis also applies to greedy recovery algorithms for which there exist universal performance bounds involving $\|\mathbf{x} - \mathbf{x}_k\|_1$. This class of algorithms includes regularized orthogonal matching pursuit (ROMP) [18] and CoSaMP [19].

III. Bounds on Confidence Interval for mode identification

A. The degeneration of k-term approximation

Theorem 1: Let $\mathbf{\Psi} \in \mathbb{C}^{N\times N}$ be $\mathbf{\Psi} = \mathbf{I} + \mathbf{E}$ and $\mathbf{x} = \mathbf{\Psi}\boldsymbol{\theta}$. If the entries of $\mathbf{E}$ are bounded as $|e_{mn}| \leq \epsilon$ for $n \in T_{\boldsymbol{\theta}}$, where $T_{\boldsymbol{\theta}}$ is the support of $\boldsymbol{\theta}$, then we have

$$\|\boldsymbol{\theta} - \boldsymbol{\theta}_k\|_1 - (N-k)\epsilon\|\boldsymbol{\theta}\|_1 \leq \|\mathbf{x} - \mathbf{x}_k\|_1 \leq \|\boldsymbol{\theta} - \boldsymbol{\theta}_k\|_1 + (N-k)\epsilon\|\boldsymbol{\theta}\|_1. \tag{12}$$

The upper bound is obtained when $e_{mn} = \epsilon \cdot e^{j\arg(\theta_m)}e^{-j\arg(\theta_n)}$ for $n \in T_{\boldsymbol{\theta}}$; and the lower bound is obtained when $e_{mn} = -\epsilon \cdot e^{j\arg(\theta_m)}e^{-j\arg(\theta_n)}$ for $n \in T_{\boldsymbol{\theta}}$.

Remark: Theorem 1 can be generalized to $\|\mathbf{x} - \mathbf{x}_k\|_2$ to obtain

$$\|\boldsymbol{\theta} - \boldsymbol{\theta}_k\|_2 - \sqrt{N-k}\epsilon\|\boldsymbol{\theta}\|_1 \leq \|\mathbf{x} - \mathbf{x}_k\|_2 \leq \|\boldsymbol{\theta} - \boldsymbol{\theta}_k\|_2 + \sqrt{N-k}\epsilon\|\boldsymbol{\theta}\|_1.$$

When $\mathbf{E} = \mathbf{0}$, the mismatch basis $\mathbf{\Psi} = \mathbf{\Psi}_0^{-1}\mathbf{\Psi}_1 = \mathbf{I}$, $\|\mathbf{x} - \mathbf{x}_k\|_1 = \|\boldsymbol{\theta} - \boldsymbol{\theta}_k\|_1$, and the compressed sensing procedure is still effective.

Suppose $\boldsymbol{\theta}$ is exactly k-sparse in $\mathbf{I}$, i.e., $\boldsymbol{\theta} = \boldsymbol{\theta}_k$. Then $\|\mathbf{x} - \mathbf{x}_k\|_1 \leq (N-k)\epsilon\|\boldsymbol{\theta}\|_1$ from Theorem 1. The bound is linear in the signal dimension N, the mismatch level ϵ and the ℓ_1 norm of $\boldsymbol{\theta}$. This means sparsity of $\mathbf{s}$ in the $\mathbf{\Psi}_1$ basis may not imply sparsity of $\mathbf{s}$ in the $\mathbf{\Psi}_0$ basis.

If the entries of $\mathbf{E}$ are lower bounded, then the following theorem gives a lower bound for the upper bound of the ℓ_1 norm of the error in the k-term approximation.

Theorem 2: Let $\mathbf{\Psi} = \mathbf{I} + \mathbf{E}$ and $\mathbf{x} = \mathbf{\Psi}\boldsymbol{\theta}$. If the entries of $\mathbf{E}$ are bounded as $|e_{mn}| \geq \eta$ for $n \in T_{\boldsymbol{\theta}}$, where $T_{\boldsymbol{\theta}}$ is the support of $\boldsymbol{\theta}$, then we have

$$\max_{\mathbf{E}:|e_{mn}|\geq\eta} \|\mathbf{x} - \mathbf{x}_k\|_1 \geq \|\boldsymbol{\theta} - \boldsymbol{\theta}_k\|_1 + (N-k)\eta\|\boldsymbol{\theta}\|_1 \tag{13}$$

Remark: Theorem 2 "lower bounds the upper bound" and implies that there is a possibility for the basis pursuit to fail, as the performance bound is now loose.

B. Image inversion

When combined with Theorem 1, the performance of basis pursuit (5) for noiseless recovery follows

$$\|\mathbf{x}^* - \mathbf{x}\|_1 \leq C_0\|\boldsymbol{\theta} - \boldsymbol{\theta}_k\|_1 + C_0(N-k)\epsilon_1\|\boldsymbol{\theta}\|_1, \tag{14}$$

if the entries of $\mathbf{E}$ satisfy $|e_{mn}| \leq \epsilon_1$. For noisy recovery (6) where $\|\mathbf{b}\|_2 \leq \epsilon_2$, the bound becomes

$$\|\mathbf{x}^* - \mathbf{x}\|_2 \leq C_0 k^{-1/2}\|\boldsymbol{\theta} - \boldsymbol{\theta}_k\|_1 + C_0(N-k)k^{-1/2}\epsilon_1\|\boldsymbol{\theta}\|_1 + C_1\epsilon_2. \tag{15}$$

We are interested in recovering $\boldsymbol{\theta}$, and the following theorem concerns the ℓ_1 error $\|\mathbf{x}^* - \boldsymbol{\theta}\|_1$ and the ℓ_2 error $\|\mathbf{x}^* - \boldsymbol{\theta}\|_2$.

Theorem 3: For noiseless basis pursuit (5), with $\delta_{2k}^{\mathbf{A}} < \sqrt{2} - 1$, we have

$$\|\mathbf{x}^* - \boldsymbol{\theta}\|_1 \leq C_0'\|\boldsymbol{\theta} - \boldsymbol{\theta}_k\|_1 + C_1'\|\boldsymbol{\theta}\|_1 \tag{16}$$

where $C_0' = C_0$ and $C_1' = [C_0(N-k) + N]\,\epsilon_1$. For noisy recovery (6) where $\|\mathbf{b}\|_2 \leq \epsilon_2$, we have

$$\|\mathbf{x}^* - \boldsymbol{\theta}\|_2 \leq C_0' k^{-1/2}\|\boldsymbol{\theta} - \boldsymbol{\theta}_k\|_1 + C_1''\|\boldsymbol{\theta}\|_1 + C_1\epsilon_2 \tag{17}$$

where $C_1'' = \left[C_0(N-k)k^{-1/2} + \sqrt{N}\right]\epsilon_1$, and C_0, C_1 are given by (11).

Remark: When $\boldsymbol{\theta}$ is exactly k-sparse, the normalized error bound for the noiseless case is

$$\frac{\|\mathbf{x}^* - \boldsymbol{\theta}\|_1}{\|\boldsymbol{\theta}\|_1} \leq C_0'\frac{\|\boldsymbol{\theta} - \boldsymbol{\theta}_k\|_1}{\|\boldsymbol{\theta}\|_1} + C_1' = C_1'. \tag{18}$$

Figure 1 illustrates the interplay between the theorems, when $\eta \leq |e_{mn}| \leq \epsilon$ for $n \in T_{\boldsymbol{\theta}}$, in the case where $\boldsymbol{\theta}$ is k-sparse and no noise is present. We aim to invert for $\boldsymbol{\theta}$ with the estimator $\mathbf{x}^*$, using the basis pursuit algorithm. From Theorem 3, we have the confidence diamond (outer diamond). However, this confidence diamond is not smaller than the inner diamond. This follows from combining Theorems 2 and 3 to find a lower bound for the upper bound on $\|\mathbf{x}^* - \boldsymbol{\theta}\|_1$. In the figure, $\boldsymbol{\theta}$ is the true parameter, $\mathbf{x}^*$ is its estimate, and $B(\epsilon) = [C_0(N-k) + N]\,\epsilon$.

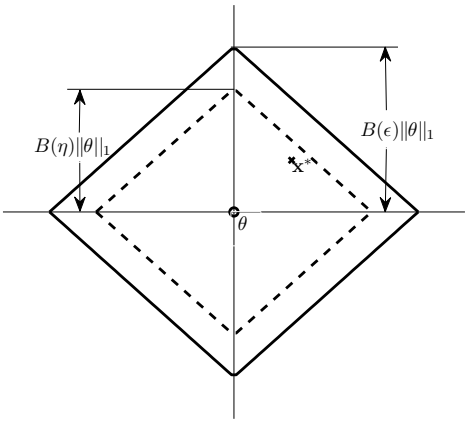

Fig. 1. Demonstration of the confidence diamond, and its lower bound, for image inversion when $\eta \leq |e_{mn}| \leq \epsilon$ for $n \in T_{\boldsymbol{\theta}}$.

IV. Modal Analysis

In spectrum analysis from compressed measurements, the signal of interests is usually assumed to be sparse on a pre-defined DFT grid. A mismatch case of particular interest is when the signal has frequency components not exactly on the DFT grid. The unitary DFT basis $\mathbf{D}_N = \boldsymbol{\Psi}_0$ can be written as

$$\mathbf{D}_N = \frac{1}{\sqrt{N}} \begin{bmatrix} 1 & 1 & \cdots & 1 \\ 1 & e^{j\frac{2\pi}{N}} & \cdots & e^{j\frac{2\pi(N-1)}{N}} \\ \vdots & \vdots & \ddots & \vdots \\ 1 & e^{j\frac{2\pi}{N}(N-1)} & \cdots & e^{j\frac{2\pi(N-1)}{N}(N-1)} \end{bmatrix}. \quad (19)$$

Without loss of generality, we assume that the tth column of the basis is mismatched by frequency $\Delta\theta$ with $0 \leq \Delta\theta \leq \frac{2\pi}{N}$ and/or a damping factor of $\lambda \leq 0$. Then $\boldsymbol{\Psi}_1 = \tilde{\mathbf{D}}_N$ is given by

$$\tilde{\mathbf{D}}_N = \mathbf{D}_N + \frac{1}{\sqrt{N}} \left(\begin{bmatrix} 1 \\ e^{\lambda + j(\frac{2\pi t}{N} + \Delta\theta)} \\ \vdots \\ e^{(\lambda + j(\frac{2\pi t}{N} + \Delta\theta))(N-1)} \end{bmatrix} - \begin{bmatrix} 1 \\ e^{j\frac{2\pi t}{N}} \\ \vdots \\ e^{j\frac{2\pi t}{N}(N-1)} \end{bmatrix} \right) \otimes \mathbf{I}(t)^T \quad (20)$$

where $\mathbf{I}(t)$ is the tth column of $\mathbf{I}$ and $\otimes$ is Kronecker product. Therefore, the corresponding mismatched basis $\boldsymbol{\Psi}$ is

$$\boldsymbol{\Psi} = \mathbf{D}_N^H \tilde{\mathbf{D}}_N = \mathbf{I} + \left(\mathbf{U}^t \begin{bmatrix} \delta_0 - 1 \\ \delta_1 \\ \vdots \\ \delta_{N-1} \end{bmatrix} \right) \otimes \mathbf{I}(t)^T \triangleq \mathbf{I} + \mathbf{E} \quad (21)$$

where $\mathbf{U}$ is an upper shift matrix and δ_m's, $m = 0, \ldots, N-1$ are samples of the Lanczos kernal at $f_m = \left(\Delta\theta - \frac{2\pi m}{N}\right) - j\lambda$ points, that is,

$$\delta_m = \frac{1}{N} \sum_{n=0}^{N-1} e^{jnf_m} = \frac{1}{N} e^{-jf_m(\frac{N-1}{2})} \frac{\sin(Nf_m/2)}{\sin(f_m/2)}. \quad (22)$$

V. Numerical Simulations

Our simulated experiments fall into two categories: those for which DFT, compressed sensing (CS), and linear prediction (LP) inversion are implemented on noise-free data, and those for which they are implemented on noisy data. For each experiment, DFT, CS, and LP are used to invert a signal or image for the underlying field parameters that gave rise to the image. Moreover, for each of these experiments DFT, CS, and LP solutions are given for the case where there is no mismatch between the assumed basis and the basis that generated the image from the field, and for the case where there is mismatch. Of course this mismatch has no influence on LP, which inverts for the modes, but it impacts DFT and CS. The effect on DFT is predictable, based on our understanding of leakage through the Lanczos kernel. The effect on CS is not well understood, and in fact our motivation is to understand it. All CS experiments are performed using the the ℓ_1 magic toolbox available online [20].

In each of Figs. 2 through 4, and 6, there are panels (a), (b), and (c). Within each of these panels are 4 subpanels: in the top-left subpanel the true underlying modes are illustrated with stems whose locations on the closed unit disc indicate the frequency and phase of the mode, and whose height illustrate the mode amplitude. The phases of the modes are randomly chosen, and not indicated on the figures. In the matched cases of panel (a), the modes are located on the rim of the unit disc at DFT frequencies. In the mismatched cases of panels (b) and (c) the modes are displaced from the DFT frequencies or they are moved off the unit circle into the interior of the disc, to damp them. In Fig. 5, the subpanels show CS inversions for field parameters, for various quadratic constraints (various values for ϵ in (6)) on the reconstruction of the recorded image. These experimental results are not an artifact of the quadratic constraint allowed or the choice of rows in the compressed recording matrix, as we have experimented with many values and reported typical results.

In all the experiments, the dimension of the image $N = 64$. The number of recordings or measurements varies from $M = 64$ to $M = 32$ to $M = 16$. For DFT and LP these recordings are actually taken at a small number of points on the image. For compressed sensing, these recordings are taken as linear combinations of all N points of the image. The order selected for all LP inversions in the noise free cases is 8. In the noisy case, the order is changed to 16 and rank reduction is applied to reduce the order to 8. The matched frequencies at which modes are placed, and their amplitudes, are $(2\pi \cdot 9/N, 1)$, $(2\pi \cdot 10/N, 1)$, $(2\pi \cdot 20/N, .5)$, and $(2\pi \cdot 45/N, .2)$ in the noise free case, and they are $(2\pi \cdot 9/N, 1)$, $(2\pi \cdot 11/N, 1)$, $(2\pi \cdot 20/N, .5)$, and $(2\pi \cdot 45/N, .2)$. For frequency mismatch, the first two modes are moved to $(2\pi \cdot 9.25/N, 1)$ and $(2\pi \cdot 9.75/N, 1)$ in the noise-free case, and to $(2\pi \cdot 9.25/N, 1)$ and $(2\pi \cdot 10.75/N, 1)$ in the noisy case. For damping mismatch the mode at $(2\pi \cdot 9/N, 1)$ is drawn off the unit circle to radius 0.95, so that the mode is damped as $(0.95)^n$. We review our findings by annotating Figs. 2-6 in the captions of the figures.

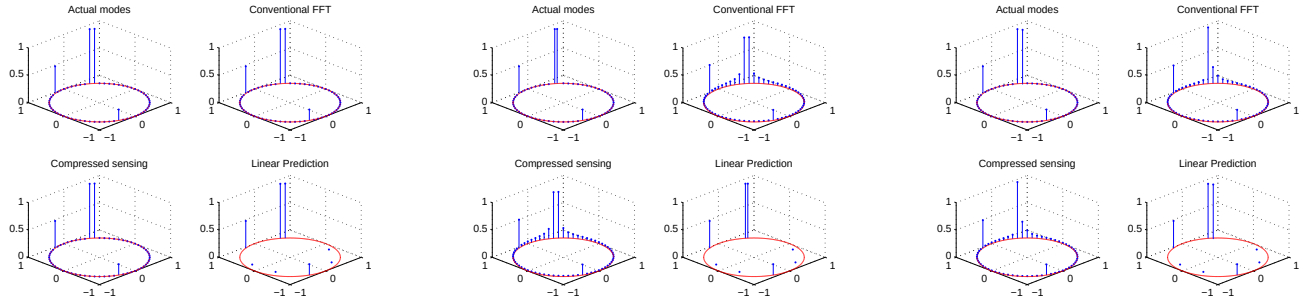

(a) No mismatch (b) Frequency mismatch (c) Damping mismatch

Fig. 2. *Full Measurements ($M = N = 64$). No Noise*. Panel (a) shows that all methods invert for the correct field, with no mismatch. Panels (b) and (c) show that with mismatch DFT and CS show comparable leakage, whereas LP is exact.

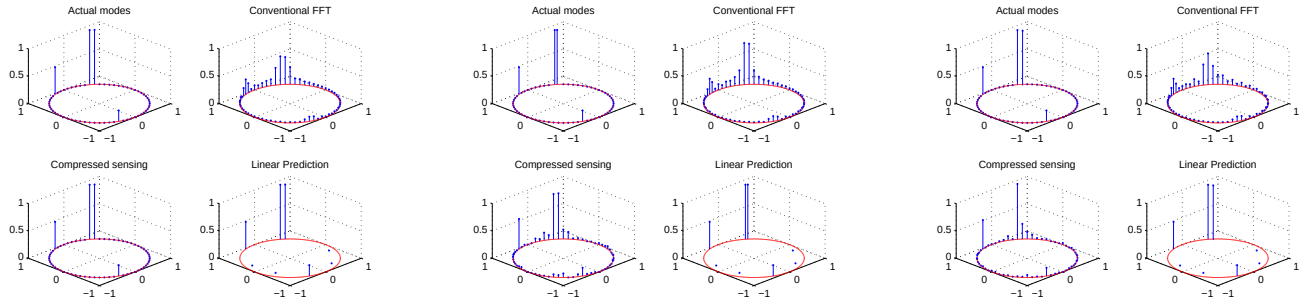

(a) No mismatch (b) Frequency mismatch (c) Damping mismatch

Fig. 3. *Compression or Recording at Half Rate ($M = N/2 = 32$). No noise*. Panel (a) shows loss of resolution in DFT, which uses a subset of samples, but exact inversion by CS, using compressed recording of all samples, and exact inversion for LP, which uses a subset of samples, with no mismatch. Panels (b) and (c) show that with mismatch, DFT and CS show comparable leakage, but LP is exact.

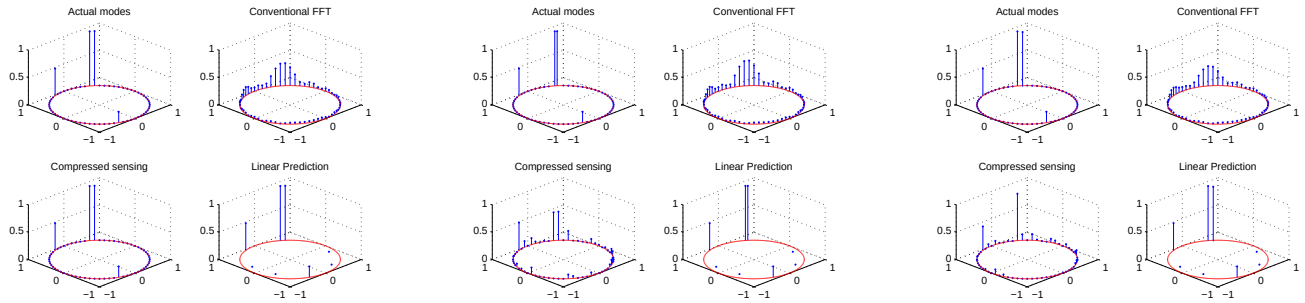

(a) No mismatch (b) Frequency mismatch (c) Damping mismatch

Fig. 4. *Compression or Recording at Quarter Rate ($M = N/4 = 16$). No noise*. Panel (a) shows loss of resolution in DFT, but exact inversion by CS and LP, with no mismatch. Panels (b) and (c) show that with mismatch DFT shows leakage, CS shows erratic inversion, and LP is exact.

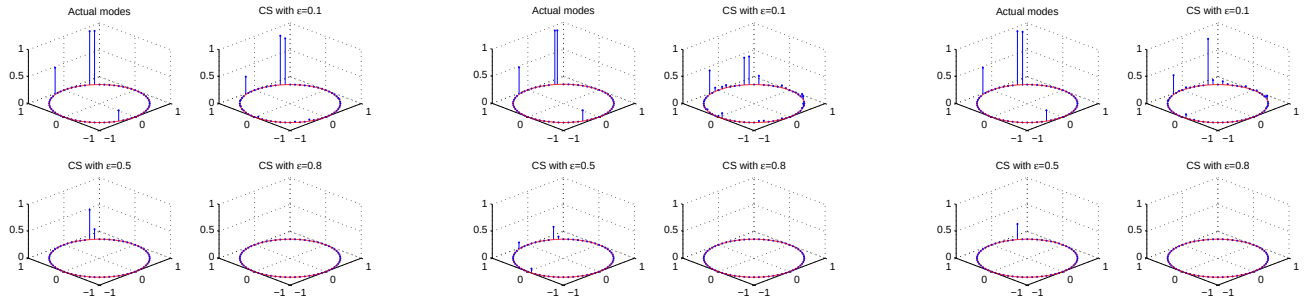

(a) No mismatch (b) Frequency mismatch (c) Damping mismatch

Fig. 5. *Compression or Recording at Quarter Rate ($M = N/4 = 16$). No Noise. Variable Quadratic Constraint for CS*. Panels (a) through (c) show performance of CS as the quadratic performance function is relaxed from $\epsilon = 0.1$ to $\epsilon = 0.8$, demonstrating that for large reconstruction errors the inversion vanishes.

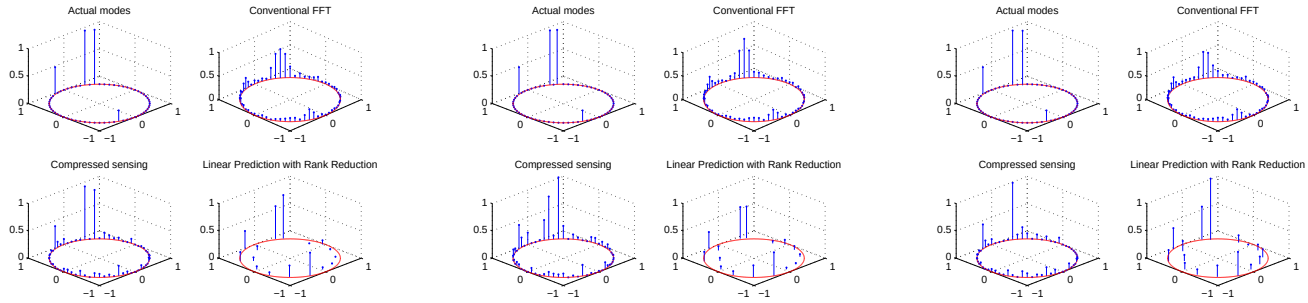

(a) No mismatch (b) Frequency mismatch (c) Damping mismatch

Fig. 6. *Compression or Recording at Half Rate ($M = N/2 = 32$). With Noise*. The DFT and LP inversions are reasonably accurate, while the CS solution is not, under conditions of no mismatch or mismatch.

VI. Appendix

A. Linear prediction for modal analysis

The problem of modal decomposition can be put in the form of an ARMA model, where the measurement record $\mathbf{y} = [y_1, \cdots, y_M]^T$ may be interpreted as a snapshot of the impulse response for an ARMA$(p, p-1)$ discrete-time system. Assume $\mathbf{y}$ can be represented by a sum of p modes, i.e.

$$y_t = \sum_{i=1}^{p} b_i z_i^{t-1}, \quad t = 1, \cdots, M \tag{23}$$

From the complex poles, form the polynomial $A(z)$:

$$A(z) = \prod_{i=1}^{p} (1 - z_i z^{-1}) = \sum_{i=0}^{p} a_i z^{-i}, \quad a_0 = 1 \tag{24}$$

Given $\mathbf{y}$, first solve the following homogeneous equation to get $\{a_i\}_{i=1}^p$:

$$\begin{bmatrix} y_1 & y_2 & \cdots & y_{p+1} \\ y_2 & y_3 & \cdots & y_{p+2} \\ \vdots & \vdots & \ddots & \vdots \\ y_{M-p} & y_{M-p+1} & \cdots & y_M \end{bmatrix} \begin{bmatrix} a_p \\ \vdots \\ a_1 \\ 1 \end{bmatrix} = \mathbf{0} \tag{25}$$

From $A(z)$, solve $\{z_i\}_{i=1}^p$ for the zeros of $A(z)$. Then $\{b_i\}_{i=1}^p$ is the solution to the linear regression problem below:

$$\mathbf{y} = \begin{bmatrix} y_1 \\ y_2 \\ \vdots \\ y_M \end{bmatrix} = \begin{bmatrix} 1 & 1 & \cdots & 1 \\ z_1 & z_2 & \cdots & z_p \\ \vdots & \vdots & \ddots & \vdots \\ z_1^{M-1} & z_2^{M-1} & \cdots & z_p^{M-1} \end{bmatrix} \begin{bmatrix} b_1 \\ b_2 \\ \vdots \\ b_p \end{bmatrix} = \mathbf{V}\mathbf{b}. \tag{26}$$

VII. Conclusions

Classical approaches to image inversion for field parameters in radar, sonar, and spectrum analysis suggest the inversion of an image using matched filtering or linear prediction. Any subsampling or compressed recording of the image has consequences for resolution (or bias) and for variability (or variance). The theory of compressed sensing suggests that compressed recording has manageable consequences, provided the image is sparse in an apriori known basis, e.g., a DFT basis or a basis associated with a range-Doppler-wavenumber grid. But no physical field is sparse in the DFT basis or in a basis defined by a regular grid in delay, doppler, frequency, and/or wavenumber.

In this paper we have investigated the sensitivity of compressed sensing (specifically basis pursuit) to mismatch between the assumed basis for sparsity and the actual sparsity basis. Our mathematical analysis and numerical examples indicate that the performance of compressed sensing for reconstructing a sparse physical field degrades considerably in the presence of mismatch, even when the assumed basis corresponds to an extremely fine-grained discretization of the parameter space. The conclusion at this point is that for high resolution spectrum analysis, DOA estimation, or delay-doppler imaging, where the problem is to identify a small number of modal parameters, rather than to reconstruct the sparsely-generated image, compressed sensing requires more study and refinement, at least for problem sizes typical in radar and sonar.

To assume that the basis for sparsity is known apriori is to assume away the very crux of image inversion, which is to *identify* the actual source modes rather than to select them from a presumed set. In fact it appears that the aims of compressed sensing are nearer to the aims of subset selection in regression analysis and order determination in linear models (see e.g. [21]) than they are to image inversion for sparse field components.

In summary, image inversion is fundamentally more challenging than image reconstruction from compressed measurements precisely because there are so many inversions that reconstruct the image. Moreover even when compressed sensing is applicable it requires a "full field of view" (a full set of image samples) which is then compressed into a small number of measurements.

References

[1] C. T. Mullis and L. L. Scharf, "Quadratic estimators of the power spectrum," in *Advances in Spectrum Estimation*, S. Haykin, Ed. Prentice Hall, 1990, vol. 1, ch. 1, pp. 1–57.

[2] H. L. Van Trees, *Optimum Array Processing*. Wiley Interscience, 2002.

[3] J. Ward, "Maximum likelihood angle and velocity estimation with space-time adaptive processing radar," in *Conf. Rec. 1996 Asilomar Conf. Signals, Systs., Comput.*, November 1996.

[4] R. Klemm, *Space-Time Adaptive Processing*. IEEE Press, 1998.

[5] L. L. Scharf, *Statistical Signal Processing*. MA: Addison-Wesley, 1991, pp. 330–331.

[6] G. H. Golub and C. F. Van Loan, *Matrix Computations*, 3rd ed. Baltimore, MD: John Hopkins Univ. Press, 1996.

[7] H. L. V. Trees and K. L. Bell, *Bayesian Bounds for Parameter Estimation and Nonlinear Filtering and Tracking*. IEEE Press, 2007.

[8] L. T. McWhorter and L. L. Scharf, "Cramer-Rao bounds for deterministic modal analysis," *IEEE Trans. Signal Processing*, vol. 41, no. 5, pp. 1847–1862, May 1993.

[9] E. J. Candés, "Compressive sampling," *Proc. Int. Congress Math.*, vol. 3, pp. 1433–1452, 2006.

[10] D. L. Donoho, "Compressed sensing," *IEEE Trans. Inform. Theory*, vol. 52, no. 4, pp. 1289–1306, 2006.

[11] R. Baraniuk, "Compressive sensing," *IEEE Signal Processing Magazine*, vol. 24, no. 4, pp. 118–121, 2007.

[12] R. Baraniuk and P. Steeghs, "Compressive radar imaging," in *Proc. 2007 IEEE Radar Conf.*, Waltham, Massachusetts, Apr. 2007, pp. 128–133.

[13] M. A. Herman and T. Strohmer, "High-resolution radar via compressed sensing," *IEEE Trans. Signal Processing*, to appear 2009.

[14] A. Gurbuz, J. McClellan, and V. Cevher, "A compressive beamforming method," in *Proc. IEEE Int. Conf. on Acoustics, Speech, and Signal Processing (ICASSP)*, Las Vegas, NV, April 2008, pp. 2617–2620.

[15] Y. Chi, A. Pezeshki, L. L. Scharf, and R. Calderbank, "Sensitivity to basis mismatch of compressed sensing," *preprint*, Aug. 2009.

[16] E. J. Candés and T. Tao, "Decoding by linear programming," *IEEE Trans. Inform. Theory*, vol. 51, pp. 4203– 4215, 2005.

[17] E. J. Candés, "The restricted isometry property and its implications for compressed sensing," *Académie des Sciences*, vol. 1, no. 346, pp. 589– 592, 2008.

[18] D. Needell and R. Vershynin, "Uniform uncertainty principle and signal recovery via regularized orthogonal matching pursuit," *Foundations of Computational Mathematics*, vol. 9, pp. 317–334, 2009.

[19] D. Needell and J. Tropp, "CoSaMP: Iterative signal recovery from incomplete and inaccurate samples," *Applied and Computational Harmonic Analysis*, vol. 26, pp. 301–321, 2008.

[20] ℓ_1 MAGIC toolbox, *http://www.acm.caltech.edu/l1magic/*, 2006.

[21] R. R. Hocking and L. L. Leslie, "Selection of the best subset in regression analysis," *Technometrics*, vol. 9, pp. 537–540, 1967.